ERJ Express. Published on April 8, 2011 as doi: 10.1183/09031936.00149810

In vivo monitoring of cystic fibrosis-like lung disease in mice by volumetric computed tomography

Mark O. Wielpütz[1,2,5], Monika Eichinger[1,5], Zhe Zhou[4,5], Karin Leotta[3], Stephanie Hirtz[4,5], Sönke H. Bartling[3], Wolfhard Semmler[3], Hans-Ulrich Kauczor[2,5], Michael Puderbach[1,5,6]*, Marcus A. Mall[4,5]*

[1]Department of Radiology, German Cancer Research Center (DKFZ), Im Neuenheimer Feld 280, 69120 Heidelberg, Germany
[2]Department of Diagnostic and Interventional Radiology, University of Heidelberg, Im Neuenheimer Feld 110, 69120 Heidelberg, Germany
[3]Medical Physics in Radiology, German Cancer Research Center (DKFZ), Im Neuenheimer Feld 280, 69120 Heidelberg, Germany
[4]Division of Pediatric Pulmonology & Allergy and Cystic Fibrosis Center, Department of Pediatrics III, University of Heidelberg, Im Neuenheimer Feld 430, 69120 Heidelberg, Germany
[5]Translational Lung Research Center, 69120 Heidelberg, Germany
[6]Department of Diagnostic and Interventional Radiology with Nuclear Medicine, Thoraxklinik at the University of Heidelberg, Amalienstraße 5, 69126 Heidelberg, Germany

*These authors contributed to this work equally.

Running title: VCT of CF-like lung disease in mice

Correspondence should be addressed to:
Prof. Dr. med. Marcus A. Mall
Division of Pediatric Pulmonology and Cystic Fibrosis Center
Department of Pediatrics III, University of Heidelberg and
Translational Lung Research Center Heidelberg
Im Neuenheimer Feld 430, 69120 Heidelberg, Germany
Tel.: +49-6221-568840
Fax: +49-6221-568806
Email: Marcus.Mall@med.uni-heidelberg.de

ABSTRACT

The onset and spontaneous development of cystic fibrosis (CF) lung disease remain poorly understood. In the present study, we used volumetric computed tomography (VCT) as a new method for longitudinal *in vivo* monitoring of early lesions and disease progression in CF-like lung disease in βENaC-transgenic (βENaC-TG) mice.

Using a VCT scanner prototype (80kV, 50mAs, scan time 19s, spatial resolution 200µm), βENaC-TG mice and wild-type (WT) littermates were examined longitudinally at 10 time points from neonatal to adult ages, and VCT images were assessed by qualitative and quantitative morphological parameters.

We demonstrate that VCT detected early onset airway mucus obstruction, diffuse infiltrates, atelectasis and air-trapping as characteristic abnormalities in βENaC-TG mice. Further, we show that early tracheal mucus obstruction predicted mortality in βENaC-TG mice and that the density of lung parenchyma was significantly reduced at all time points in βENaC-TG compared to WT mice (-558 $\pm$ 8 Hounsfield Units [HU] in WT vs. -686 $\pm$ 16 HU in βENaC-TG at 6 weeks of age; $p<0.005$).

Our study demonstrates that VCT is a sensitive non-invasive technique for early detection and longitudinal monitoring of morphological abnormalities of CF-like lung disease in mice, and may thus provide a useful tool for pre-clinical *in vivo* evaluation of novel treatment strategies for CF.

Keywords

Cystic fibrosis, lung disease, lung imaging, computed tomography, transgenic mouse model, epithelial Na^+ channel

INTRODUCTION

Cystic fibrosis (CF) lung disease is caused by mutations in the cystic fibrosis transmembrane conductance regulator (CFTR) gene and belongs to the most common lethal hereditary diseases in Caucasians [1, 2]. The hallmarks of CF lung disease are highly viscous airway secretions causing airway mucus obstruction, chronic inflammation, refractory bacterial infection, bronchiectasis and emphysema leading to progressive lung destruction and respiratory failure [3, 4].

In epithelial cells lining the airway surfaces, CFTR acts as a cAMP-dependent Cl^- channel and regulator of the epithelial Na^+ channel (ENaC) [5-8], thus regulating epithelial transport of salt and water and the height of the thin film of liquid that covers the airways (airway surface liquid, ASL). In CF airways, CFTR dysfunction results in deficient Cl^- secretion and increased ENaC-mediated Na^+ absorption producing ASL depletion and impaired mucociliary clearance [9-11]. The critical role of ASL depletion in the *in vivo* pathogenesis was confirmed in the βENaC-transgenic (βENaC-TG) mouse, which mimics increased airway Na^+ absorption and develops a CF-like lung disease characterized by high pulmonary mortality due to airway mucus obstruction and chronic inflammation, poor bacterial clearance and emphysema with distal airspace enlargement and increased lung capacity in adult survivors [12-14].

Previous studies using the βENaC-TG mouse to monitor the *in vivo* development of morphological changes in CF-like lung disease, and the use of this model for preclinical evaluation of novel therapeutic strategies, relied on post-mortem histopathology [12, 13, 15]. This approach is inherently limited by single time point observations, and no data are available from βENaC-TG mice that die spontaneously of lung disease during the observational period. Furthermore, for longitudinal studies, large numbers of mice are needed to study inter-individual lung morphology at different time points [13]. Other investigators have used micro-computed tomography (μCT) as an alternative approach to study lung morphology in murine models of interstitial lung disease and emphysema *in vivo*

and post mortem at very high resolution [16, 17]. However, μCT has not been used for longitudinal *in vivo* studies due to the wearing and potentially lethal procedure, which requires long scanning times (up to 30 min), high radiation doses and invasive anesthesia [18, 19]. Volumetric computed tomography (VCT) provides the possibility for intra-individual longitudinal imaging studies to evaluate the natural course of lung disease in individual mice *in vivo* at a spatial resolution high enough to study lung morphology in small laboratory animals [20, 21]. Instead of multidetector rows used in clinical scanners, VCT features a rotating flat-panel detector, achieving isotropic voxels of approx. 200 μm with the setup used for the present study. In contrast to μCT, VCT is less wearing for experimental animals because of shorter acquisition times (scan time approx. 19 s) and therefore lower cumulative exposure to x-rays and anaesthetics. Additionally, a large field of view allows examining multiple mice within the same scan [20-22].

The aim of this study was to evaluate VCT to monitor the onset and spontaneous progression of lung disease in βENaC-TG mice *in vivo*, and to describe radiological features of this histomorphologically well-charaterized mouse model of CF lung disease. To achieve this goal, we performed longitudinal VCT imaging studies in βENaC-TG mice and wild-type (WT) littermate controls from neonatal to adult ages, and compared airway and parenchymal morphology by qualitative evaluation of airway mucus obstruction, infiltrates, atelectasis and air-trapping, and by quantitative measurements of the lung density. Findings from VCT studies were validated by lung histology, morphometric analyses of airway mucus obstruction and distal airspace enlargement, and pulmonary function tests at selected time points.

MATERIALS AND METHODS

Experimental Animals

All animal studies were approved by the Regierungspräsidium Karlsruhe, Germany. The generation of βENaC-TG mice (line 6608) has been described previously [12]. The colony was originally established and maintained on a mixed genetic background (C3H/HeN x C57BL/6N). Experimental animals were generated by breeding of hemizygous βENaC-TG mice with C3B6 F1 wild-type mice (Charles River Laboratories, Sulzfeld, Germany) to prevent genetic drifts in the colony, and βENaC-TG mice were identified by PCR of genomic DNA as described [12, 13]. WT littermates served as controls in all experiments to control for possible effects of genetic background and environment on the phenotype. Mice were housed in a specific-pathogen-free animal facility and had free access to chow and water.

Volumetric computed tomography

A prototype VCT scanner (Siemens Medical Solutions AG, Forchheim, Germany) consisting of a flat-panel detector and a modified x-ray tube both mounted on a clinical multislice CT gantry was employed as previously described [22, 23]. The flat-panel detector (PaxScan 4030CB, Varian Medical Systems, Palo Alto, CA), poses 2048 x 1536 detector pixels on an active area of 40 x 30 cm², each with a dimension of 194^2 μm^2. The source-to-detector distance was 93.0 cm, and the source-to-isocenter distance was 57.3 cm resulting in a magnification of 1.6. The detector was read out in a 2 × 2 binning mode, meaning that four neighbouring pixels were averaged. Taking the geometry of the VCT system setup into consideration, the instrument's total field of view is 25 × 25 × 18 cm^3 at an isotropic resolution of 200 µm [22, 23]. The frame rate was 30 frames per second. Scan parameters were 80 kV and 50 mAs at a scan time of 19 s. Effective dose of a scan that employs the same scan parameters measured in air kerma was approx. 22.8 mGy [23]. Mice were placed randomly side by side in prone position for scanning in groups of 3 littermates. VCT was performed in freely breathing mice under inhalative sedation with 1 - 2 % sevoflurane (Sevorane®, Abbott, Wiesbaden, Germany) nebulized in pure O_2 (Linde, Pullach, Germany) on days 3, 5, 7, 10,

14, 17, 21, 24, 28 and 42 after birth; or immediately after death. As up to 3 mice were examined at the same time, the field of view for the reconstruction in growing mice was adopted to the individual chest diameter. Image reconstruction in transversal plane from 360° projection data was performed with a cone-beam algorithm by filtered back projection with a sharp kernel typically used for lung imaging as described previously [23].

VCT image evaluation

Evaluation of VCT images was performed by an investigator (M.O.W.) blinded for the genotype of the mice in a lung window (width 1240, center -400) (Chili Pacs® Software version 2.6, Chili GmbH, Heidelberg, Germany), using a commercially available workstation with two flat-panel screens. The software allows simultaneous image evaluation in three planes by real-time multiplanar reconstruction. This approach enables secure identification of the lesions of interest as well as partial volume effects, which is benefitial e.g. for the analysis of airway obstruction. To facilitate comparative viewing in the figures, VCT images of mice of different ages were magnified to the same size explaining the lower final resolution (relative blurring) of images shown from young mice. Scale bars were added in each image to indicate differences in lung size. Initial VCT images of mice of all ages were scanned for distinct lesions, which were used to develop a standardized database to evaluate VCT images with respect to qualitative and quantitative parameters as follows:

Qualitative assessment: Airway obstruction was assessed separately in the trachea, main stem bronchi and intrapulmonary bronchi. Partial or complete opacification of the tracheal lumen between larynx and bifurcation, main stem bronchi or intrapulmonary bronchi was rated as a positive finding. In addition to airway obstruction, each quadrant of the lung parenchyma was independently assessed for the presence of the following abnormalities: 1) diffuse infiltrates defined as diffusely distributed spotted opacities of the lung not covering a lobe or segment; 2) atelectasis defined as homogeneous opacity with volume loss that covers a lobe or segment; 3) air-trapping, which was defined as a focal sharply delineated

area of decreased density compared to encompassing parenchyma. Furthermore, overall visual appearance of the lung texture as a whole was classified as homogeneous, focally inhomogeneous (showing at least one of the lesions defined above), or globally inhomogeneous.

Quantitative assessment: The density of the lung parenchyma was measured in Hounsfield Units (HU) by placing 4 circular regions of interest (ROI) with a diameter of 1 mm in both upper and lower lung regions. When placing the ROI, a representative lung area was selected randomly after excluding large airways, large vessels, infiltrates, atelectasis and air-trapping from the measurement. Based on these four measurements, the mean HU was calculated for each mouse.

Morphology

Anesthetized mice were killed by exsanguination. Lungs and tracheae were removed through a median sternotomy, fixed in 4% buffered formalin, and embedded in paraffin. Sections were cut at 5 µm and stained with hematoxylin and eosin (H&E) or Alcian blue periodic acid-Schiff (AB-PAS) as previously described [13].

Airway morphometry

Morphometric analyses of airway mucus obstruction were performed in non-inflated, immersion fixed tracheae and left lungs. Tracheae were sectioned longitudinally, and lungs were sectioned transversally at the level of the proximal intrapulmonary main axial airway near the hilus [13]. For quantitative stereological assessment of airway mucus obstruction, we used Cell^F image analysis software (Olympus GmbH, Hamburg, Germany) to determine mucus volume density as previously described [13, 24]. In brief, images of airway sections were acquired with an Olympus IX-71 microscope (Olympus GmbH, Hamburg, Germany), the length of the airway boundary, as defined by the epithelial basement membrane, was measured by the interactive image measurement tool, and the AB-PAS positive surface area

within this boundary was measured by phase analysis according to the automatic threshold settings of the software. The volume density of airway mucus, representing the volume of airway mucus content per surface area of the basement membrane (nl / mm^2), was determined from the surface areas of AB-PAS positive mucus and the basement membrane length, as previously described [13, 24].

Mean linear intercepts

Lungs from 3-day-old mice were immersion fixed in 4% buffered formalin and right lungs from 2-week-old and 6-week-old mice were inflated with 4% buffered formalin to 25 cm of fixative pressure. Subsequently, lungs were processed for histology, sectioned at 5 µm, and stained with hematoxylin and eosin (H&E). Histological images were digitally captured with an Olympus IX 71 microscope, using Cell^F image analysis software (Olympus GmbH, Hamburg, Germany) with a line counting tool at a 16 fold magnification beginning at randomly selected spots. Mean linear intercepts were determined by dividing the sum of the lengths of all lines in all frames by the number of intercepts between alveolar septi and counting lines [25]. For each animal, a minimum of 200 intercepts were sampled in 10 fields in different lobes as previously described [13].

Pulmonary function studies

To evaluate lung mechanics, 6-week-old adult mice were anesthetized with an intraperitoneal injection of ketamine and xylazine (120 mg / kg and 16 mg / kg, respectively), paralyzed with intraperitoneal injection of 0.8 mg / kg pancuroniumbromide (Inresa Arzneimittel GmbH, Freiburg, Germany), tracheostomized, and mechanically ventilated at a rate of 150 breaths / min, a tidal volume of 10 ml / kg, and a positive end-expiratory pressure of 3 cm H_2O with a computer-controlled small animal ventilator (FlexiVent system, SCIREQ Inc., Montreal, PQ, Canada). Pressure volume curves (PVs-P = PV-stepwise pressure regulated) and total lung capacity (TLC) were determined using the custom-designed FlexiVent software (SCIREQ Inc., Montreal, PQ, Canada) as previously described [26].

Statistical analysis

The data were recorded in a dedicated database (Microsoft Access, Microsoft Corp., Redmond, USA). Statistical analysis was performed with SigmaPlot® (Systat Software GmbH, Erkrath, Germany). Dichotomous data from qualitative parameters were tested pairwise using Fisher's exact test and correction for multiple testing was done by Bonferroni's method. Qualitative data are shown as percentages of mice per group presenting the lesion of interest. For quantitative data, normality testing was performed to assess whether parametric or non-parametric tests should be employed. Multiple comparisons of quantitative data obtained by VCT or morphometry at different time points in mice of the same genotype (i.e. WT or βENaC-TG) were performed using one-way analysis of variances (ANOVA) or Kruskal-Wallis ANOVA on ranks with post-hoc tests as appropriate. Statistical comparisons between mice of different genotypes (i.e. WT vs. βENaC-TG) were performed by Student's t-test or Mann-Whitney-U test and multiple comparisons were compensated for by using Bonferroni's method. Quantitative data are shown as mean or median ± SEM, or median with 25^{th} and 75^{th} percentile respectively. A p-value of $p < 0.05$ or $p < 0.05 / m$ (number of tests) for Bonferroni's method was considered statistically significant. Additionally, receiver operating characteristics (ROC) analysis was performed for HU data in order to determine a threshold that discriminates between WT and βENaC-TG mice. The positive likelihood ratio was calculated. Cut-off values with a positive likelihood ratio above 10 are generally considered reliable.

RESULTS

Development of airway mucus obstruction in βENaC-TG mice

To study the longitudinal development of airway obstruction by VCT, we evaluated images of neonatal to adult βENaC-TG mice and WT littermates for partial or complete opacification of conducting airways, including trachea (figure 1), main stem bronchi (figure 2) and intrapulmonary bronchi. In βENaC-TG mice, opacification of the trachea was a characteristic feature of early lung disease and the frequency of this lesion decreased with age (figures 1d, e and g). In contrast, tracheal obstruction was not observed by VCT in WT mice at any time point (figures 1 a, b and g). Comparative histopathological evaluation of tracheae in 3-day-old neonatal mice demonstrated that opacities detected by VCT reflected intraluminal mucus obstruction (figures 1c and f) as previously described [13]. Overall, tracheal obstruction was detected by VCT in n = 5 out of 20 βENaC-TG mice (25%) on day 3, all of which died spontaneously before the end of the study (figure 1g and h).

Subsequently, narrowing or complete obstruction of the main stem bronchi was observed by VCT in a substantial number of βENaC-TG mice and to more variable extents also in WT littermates (figures 2a, b and c and supplementary figure online). However, main stem bronchi of βENaC-TG mice were significantly more often affected than those of WT mice on day 7 ($p < 0.05$) and showed a trend towards a higher frequency of bronchial obstruction thereafter (figure 2h). This pattern detected by VCT was consistent with the pattern of intraluminal mucus obstruction of main stem bronchi detected by lung histology in βENaC-TG and WT mice. In agreement with previous studies [13], airway morphology and morphometry at selected time points of the VCT study demonstrated severe and persistent mucus obstruction in βENaC-TG mice, and a transient increase of goblet cell numbers and mucus accumulation in juvenile WT mice that peaked at the age of 2 weeks and waned thereafter (figures 2d - h). Of note, the identification of obstruction of small intrapulmonary bronchi by VCT was limited by the maximum spatial resolution (i.e. ~ 200 µm). Taken together, these data demonstrate that VCT is a sensitive technique for *in vivo* monitoring of mucus obstruction in conducting airways including trachea and main stem bronchi in mice.

βENaC-TG mice exhibit abnormalities of the lung parenchyma

Next, we performed a longitudinal evaluation of focal and generalized abnormalities of the lung parenchyma in WT and βENaC-TG mice. Figure 3 shows representative VCT images of WT and βENaC-TG mice at four different time points during lung development and provides an overview of characteristic abnormalities in βENaC-TG mice. First, we focussed on focal structural alterations of the lung parenchyma including infiltrates, atelectasis and air-trapping. In WT mice, infiltrates and atelectasis occurred only rarely and without any predilection for a specific age. Lucencies as a sign of air-trapping were not observed in WT mice and the global lung texture was homogeneous at all time points (figures 3 - 5). In contrast, diffuse infiltrates were more frequently observed in βENaC-TG compared with WT mice during the first week of life ($p < 0.05$ to $p < 0.001$), but were rarely detected thereafter (figures 4b, c and e). Signs of atelectasis were more commonly found in 1- to 3-week-old βENaC-TG mice compared to WT controls ($p < 0.05$ on day 21) (figures 4c, d and f). As shown in figure 5, air-trapping occurred in parallel with atelectasis in βENaC-TG mice, where it was most frequent at the age of 7 to 24 days (figure 5a). Moreover, βENaC-TG mice presented with a globally inhomogeneous and hypodense lung structure from day 3 onwards (figures 3 and 5b). By considering the presence of inhomogeneous parenchyma as a single parameter, βENaC-TG mice could reliably be identified by the reader ($p < 0.005$) (figure 5b).

Development of emphysema in βENaC-TG mice

In addition to qualitative assessment of the lung texture by VCT, we quantified the lung density of WT and βENaC-TG mice by measuring the CT density in Hounsfield Units (HU). In WT mice, these measurements revealed an increase in median HU during the first days of life, with a peak at day 10 compared to day 3 after birth ($p < 0.05$) (figure 6a). After this peak, the density continuously decreased until the age of 42 days, when tissue density was significantly reduced compared to juvenile (5-day-old to 10-day-old) WT mice ($p < 0.05$). In βENaC-TG mice, HU were significantly lower than in age-matched WT mice at all time points

($p < 0.005$). Further, tissue density failed to increase in βENaC-TG mice during the first week of life, but decreased continuously from day 3 to day 42 ($p < 0.05$). As a consequence, the difference in lung density between βENaC-TG and WT mice increased from the first to the last scan. On day 3, the difference in median HU between WT and βENaC-TG mice was 60 $\pm$ 20 HU, and this gap increased significantly to 129 $\pm$ 16 HU on day 42 ($p < 0.05$). ROC analysis revealed that as early as day 3, WT and βENaC-TG mice can be discriminated by a cut-off value of -552 HU with a sensitivity of 79%, a specificity of 95% and a positive likelihood ratio (+LR) of 15.8. On day 42, sensitivity and specificity were calculated 92% and 91%, respectively, and +LR 10.1 for a cut-off of –605 HU. Taken together, these results demonstrate substantial changes in parenchymal density during normal lung development in WT mice, and identified reduced tissue density characteristic of emphysema as an early and persistent abnormality in lungs from βENaC-TG mice. To validate these findings from VCT studies by independent measurements, we determined mean linear intercepts as a parameter for alveolar diameter at selected time points (i.e. at 3, 14 and 42 days of age) (figure 6b). These measurements demonstrated that reduced tissue density, as determined from Hounsfield Units by VCT (figure 6a), was associated with significant enlargement of distal airspaces at all time points in βENaC-TG mice compared to WT littermates ($p < 0.017$) (figures 6b, c and d). Further, pulmonary function testing demonstrated a significant upwards shift of pressure volume curves ($p < 0.01$) and a significant increase in total lung capacity (TLC) ($p < 0.05$) characteristic of emphysema [26] in adult βENaC-TG compared to wild-type mice (figures 6e and f). Collectively, these data demonstrate that βENaC-TG mice develop early onset emphysema and that VCT is a sensitive imaging modality to monitor emphysema development *in vivo*.

DISCUSSION

Lung disease in CF patients is characterized by various, often co-existing lesions including airway mucus plugging, atelectasis, infiltration and emphysema [2-4]. However, little is known about initial lesions and spontaneous development of disease *in vivo* and currently, no therapies are available that target CF lung disease at its root cause. The βENaC-TG mouse mimics basic CF airway defects (i.e. increased airway Na^+ absorption and ASL depletion) and phenocopies CF lung disease providing an opportunity for studies of the *in vivo* pathogenesis and preclinical evaluation of novel therapeutic strategies [12, 13, 15, 27]. Previous studies with this mouse model of CF lung disease provided a detailed histomorphological characterization of airway mucus obstruction and emphysema [12, 13], but the onset and spontaneous progression of these morphological changes have not been studied *in vivo*.

In this study, we therefore used VCT to analyse the development and spontaneous progression of CF-like lung disease in βENaC-TG mice and validated data obtained from VCT studies by histomorphological studies and pulmonary function testing at selected time points. In agreement with previous histology studies [13] and histomorphological data from this study (figures 1 and 2), VCT imaging detected a high incidence of tracheal opacification reflecting early mucus plugging of the trachea in the neonatal period, and progression of airway mucus obstruction into the lower airways of βENaC-TG mice in the first weeks of life. Of note, early postnatal obstruction of the trachea was only observed in βENaC-TG, but not in WT mice, and was a strong predictor of subsequent death of affected mice. The inter- and intra-individual variability of airway obstruction observed between different time points suggests that airway narrowing detected by VCT reflected variable obstruction due to intraluminal accumulation of mucus in airways of βENaC-TG mice.

In addition to airway mucus obstruction, VCT depicted several structural abnormalities of the lung parenchyma in βENaC-TG mice that were not appreciated in previous

histomorphological studies. In general, focal structural abnormalities of the lung, subdivided into diffuse infiltrates, atelectasis, and air-trapping were significantly more frequent in βENaC-TG mice compared to WT littermates (figures 4 and 5). Regarding the timing of occurrence of these abnormalities during development, we speculate that the early appearance of diffuse infiltrates in βENaC-TG mice may be a consequence of central mucus plugging in the trachea leading to a more global impairment of ventilation [13]. Conversely, we speculate that the later onset of atelectasis and air-trapping (figures 4 and 5) reflects a more regional pattern of mucus obstruction of intrapulmonary bronchi in βENaC-TG mice beyond the first week of life (figure 2).

Furthermore, we detected a significantly reduced tissue density (figure 6a) and global parenchymal inhomogeneity (figure 5b) in βENaC-TG compared to WT mice at all stages. In WT mice, HU increased significantly until day 10, likely reflecting the process of alveolar septation leading to an increase in tissue density during early postnatal development [28]. Subsequently, parenchymal tissue density gradually decreased, as expected during growth of the thorax and concomitant distension of distal airspaces. In βENaC-TG mice, parenchymal density was significantly reduced at all time points studied, and the difference in tissue density between βENaC-TG and WT mice increased with age during the observational period. Interestingly, the difference in lung density between WT and βENaC-TG mice was similar to the difference recently observed between COPD patients with emphysema and controls [29] indicating that βENaC-TG mice develop emphysema to a level that is pathophysiologically relevant in humans. Reduced parenchymal tissue density in βENaC-TG was associated with early onset distal airspace enlargement, as determined from measurements of mean linear intercepts in neonatal to adult mice (figure 6d). Further, pulmonary function tests detected abnormalities characteristic of emphysema such as an upwards shift of pressure volume curves and increased total lung capacity (TLC) [26] in βENaC-TG mice compared with WT littermates (figures 6e and f). Taken together, these data obtained from VCT imaging, alveolar morphology and lung function testing, demonstrated

that early onset and progressive emphysema is a characteristic abnormality in βENaC-TG mice.

Regarding the mechanism of emphysema formation, we speculate that several factors including 1) impaired postnatal alveolarization, 2) persistent air-trapping due to mucus obstruction leading to irreversible mechanical over-distention of distal airspaces, and 3) a protease/anti-protease imbalance resulting from chronic inflammation associated with recruitment of macrophages and neutrophils, and elevated levels of pro-inflammatory cytokines may contribute to the early development of this abnormality in βENaC-TG mice [13]. In this context, ongoing studies indicate that airway surface dehydration may cause activation of macrophages by particulates or irritants that are not properly cleared from mucostatic airways causing elevated expression of macrophage elastase (MMP12), which may be implicated in emphysema formation in βENaC-TG mice [30-32]. Of note, besides small airway mucus obstruction early onset emphysema has been reported as an early and invariable feature in the lungs of CF infants who died in the first year of life [3], highlighting the clinical importance of this phenotype in CF patients. Our studies demonstrate that VCT imaging provides a powerful tool for *in vivo* monitoring of emphysema in mice. We expect that this non-invasive endpoint will help to further elucidate the mechanisms underlying emphysema formation in CF and other chronic lung diseases in future preclinical studies including genetic and pharmacologic approaches.

Our data demonstrate that longitudinal *in vivo* imaging by VCT has significant advantages over a cross-sectional histopathological approach for phenotyping of lung disease in mice. First, VCT enabled intra-individual monitoring of the development of specific abnormalities in βENaC-TG mice (figures 1, 2, 4 - 6). Further, longitudinal VCT imaging allowed us to study morphological changes that occurred in deceased βENaC-TG mice prior to death, and thus capture valuable information that cannot be obtained by histopathological evaluation. Moreover, VCT provides images of the lung as a whole, whereas histology is typically limited

to a small number of lung sections. Finally, by exploiting these advantages, VCT has the potential to reduce the number of experimental mice required for future studies with morphological outcomes.

In vivo imaging of the lung of small laboratory animals by VCT has several advantages when compared to other imaging techniques. In previous studies, µCT was used to provide high-resolution images with possible voxel sizes below 50 µm [18, 19, 33] to study murine models of interstitial lung disease and emphysema [16, 17]. However, µCT requires long scanning times of up to 30 min [17] accompanied by high radiation exposure of up to several Gy [33], and invasive anaesthesia. Thus, there is agreement that the usefulness of µCT for longitudinal *in vivo* studies is limited [19, 33]. Other investigators employed magnetic resonance imaging (MRI) for visualization of the pleura and gross pulmonary fluid in rat models for pulmonary inflammation [34, 35]. However, the limited spatial resolution of MRI precludes its use for structural analysis of airways and lung parenchyma in small laboratory animals.

Because the lung has a high inherent tissue contrast, we applied higher photon energies (80 kV) and reduced scan times to several seconds. Using these settings, we demonstrate that the resolution achieved by VCT was sufficient to identify alterations of the lung texture and the larger airways already in 3-day-old neonatal mice with a body weight of ~2 to 3 g. The maximum cumulative dose of 10 subsequent VCT scans was approximately 230 mGy [23], which was well tolerated by mice in our as well as in previous studies [36, 37], thus allowing non-invasive longitudinal monitoring of lung disease in mice from neonatal to adult ages.

Our study also indentified some limitations of VCT in pulmonary imaging of mice. Because the diameter of small airways [38] is below the spatial resolution of VCT [22], the technique was insensitive to detect abnormalities in this airway region. Moreover, cardiac and respiratory motion of freely breathing mice likely decreased the signal-to-noise ratio.

However, we decided against the use of respiratory or cardiac gating in our experiments [22] for the following reasons: Most lung alterations of interest in this study affected the organ as a whole, whereas gating for VCT was described to increase mainly the delineation of structures close to the diaphragm [22]. Therefore, the additional scan time, x-ray exposure and anaesthetics required for retrospective gating may have adverse effects on animal survival and lung structure, without providing relevant additional information. Second, simultaneous scanning of several animals allowed studies of larger groups, but made gating of respiratory and cardiac function impossible.

In summary, we demonstrate that VCT imaging is suitable to detect key histopathological features, such as airway mucus obstruction and emphysema in βENaC-TG mice. Further, VCT studies identified additional abnormalities, which were previously not appreciated by histopathological evaluation, but represent common morphological changes in lung disease in patients with CF including pulmonary infiltrates, atelectasis and air-trapping. We conclude that VCT is a sensitive technique for longitudinal non-invasive monitoring of small animal models of CF and potentially other lung diseases associated with changes in parenchymal density, atelectasis, infiltration or emphysema, such as pneumonia, bronchopulmonary dysplasia and chronic obstructive pulmonary disease (COPD). In these disease models, we predict that VCT will provide a valuable tool for studies of the *in vivo* pathogenesis and may serve as an endpoint for preclinical evaluation of novel therapeutic strategies.

SUPPORT STATEMENT

This study was supported by the Deutsche Forschungsgemeinschaft (DFG MA 2081/3-2 and MA 2081/4-1) and the European Commission (MEXT-CT-2004-013666).

ACKNOWLEDGEMENTS

We thank Jolanthe Schatterny for expert technical assistance in genotyping of experimental animals.

REFERENCES

1. Kerem B, Rommens JM, Buchanan JA, Markiewicz D, Cox TK, Chakravarti A, Buchwald M, Tsui LC. Identification of the cystic fibrosis gene: genetic analysis. *Science* 1989: 245(4922): 1073-1080.

2. Welsh MJ, Ramsey B. W., Accurso F., Cutting G. R., ed. Cystic Fibrosis. 8th ed. McGraw Hill, New York, 2001.

3. Zuelzer WW, Newton WA, Jr. The pathogenesis of fibrocystic disease of the pancreas; a study of 36 cases with special reference to the pulmonary lesions. *Pediatrics* 1949: 4(1): 53-69.

4. Gibson RL, Burns JL, Ramsey BW. Pathophysiology and management of pulmonary infections in cystic fibrosis. *Am J Respir Crit Care Med* 2003: 168(8): 918-951.

5. Canessa CM, Schild L, Buell G, Thorens B, Gautschi I, Horisberger JD, Rossier BC. Amiloride-sensitive epithelial Na+ channel is made of three homologous subunits. *Nature* 1994: 367(6462): 463-467.

6. Stutts MJ, Canessa CM, Olsen JC, Hamrick M, Cohn JA, Rossier BC, Boucher RC. CFTR as a cAMP-dependent regulator of sodium channels. *Science* 1995: 269(5225): 847-850.

7. Mall M, Hipper A, Greger R, Kunzelmann K. Wild type but not deltaF508 CFTR inhibits Na+ conductance when coexpressed in Xenopus oocytes. *FEBS Lett* 1996: 381(1-2): 47-52.

8. Mall M, Bleich M, Greger R, Schreiber R, Kunzelmann K. The amiloride-inhibitable Na+ conductance is reduced by the cystic fibrosis transmembrane conductance regulator in normal but not in cystic fibrosis airways. *J Clin Invest* 1998: 102(1): 15-21.

9. Matsui H, Grubb BR, Tarran R, Randell SH, Gatzy JT, Davis CW, Boucher RC. Evidence for periciliary liquid layer depletion, not abnormal ion composition, in the pathogenesis of cystic fibrosis airways disease. *Cell* 1998: 95(7): 1005-1015.

10. Knowles MR, Boucher RC. Mucus clearance as a primary innate defense mechanism for mammalian airways. *J Clin Invest* 2002: 109(5): 571-577.

11. Mall MA. Role of cilia, mucus, and airway surface liquid in mucociliary dysfunction: lessons from mouse models. *J Aerosol Med Pulm Drug Deliv* 2008: 21(1): 13-24.

12. Mall M, Grubb BR, Harkema JR, O'Neal WK, Boucher RC. Increased airway epithelial Na+ absorption produces cystic fibrosis-like lung disease in mice. *Nat Med* 2004: 10(5): 487-493.

13. Mall MA, Harkema JR, Trojanek JB, Treis D, Livraghi A, Schubert S, Zhou Z, Kreda SM, Tilley SL, Hudson EJ, O'Neal WK, Boucher RC. Development of chronic bronchitis and emphysema in beta-epithelial Na+ channel-overexpressing mice. *Am J Respir Crit Care Med* 2008: 177(7): 730-742.

14. Mall MA. Role of the amiloride-sensitive epithelial Na+ channel in the pathogenesis and as a therapeutic target for cystic fibrosis lung disease. *Exp Physiol* 2009: 94(2): 171-174.

15. Zhou Z, Treis D, Schubert SC, Harm M, Schatterny J, Hirtz S, Duerr J, Boucher RC, Mall MA. Preventive but not late amiloride therapy reduces morbidity and mortality of lung disease in betaENaC-overexpressing mice. *Am J Respir Crit Care Med* 2008: 178(12): 1245-1256.

16. Postnov AA, Meurrens K, Weiler H, Van Dyck D, Xu H, Terpstra P, De Clerck NM. In vivo assessment of emphysema in mice by high resolution X-ray microtomography. *J Microsc* 2005: 220(Pt 1): 70-75.

17. Lee HJ, Goo JM, Kim NR, Kim MA, Chung DH, Son KR, Kim HC, Lee CH, Park CM, Chun EJ, Im JG. Semiquantitative measurement of murine bleomycin-induced lung fibrosis in in vivo and postmortem conditions using microcomputed tomography: correlation with pathologic scores--initial results. *Invest Radiol* 2008: 43(6): 453-460.

18. Ritman EL. Micro-computed tomography-current status and developments. *Annu Rev Biomed Eng* 2004: 6: 185-208.

19. Ritman EL. Micro-computed tomography of the lungs and pulmonary-vascular system. *Proc Am Thorac Soc* 2005: 2(6): 477-480, 501.

20. Kiessling F, Greschus S, Lichy MP, Bock M, Fink C, Vosseler S, Moll J, Mueller MM, Fusenig NE, Traupe H, Semmler W. Volumetric computed tomography (VCT): a new

technology for noninvasive, high-resolution monitoring of tumor angiogenesis. *Nat Med* 2004: 10(10): 1133-1138.

21. Greschus S, Kiessling F, Lichy MP, Moll J, Mueller MM, Savai R, Rose F, Ruppert C, Gunther A, Luecke M, Fusenig NE, Semmler W, Traupe H. Potential applications of flat-panel volumetric CT in morphologic and functional small animal imaging. *Neoplasia* 2005: 7(8): 730-740.

22. Bartling SH, Stiller W, Grasruck M, Schmidt B, Peschke P, Semmler W, Kiessling F. Retrospective motion gating in small animal CT of mice and rats. *Invest Radiol* 2007: 42(10): 704-714.

23. Gupta R, Grasruck M, Suess C, Bartling SH, Schmidt B, Stierstorfer K, Popescu S, Brady T, Flohr T. Ultra-high resolution flat-panel volume CT: fundamental principles, design architecture, and system characterization. *Eur Radiol* 2006: 16(6): 1191-1205.

24. Harkema JR, Plopper CG, Hyde DM, St George JA. Regional differences in quantities of histochemically detectable mucosubstances in nasal, paranasal, and nasopharyngeal epithelium of the bonnet monkey. *J Histochem Cytochem* 1987: 35(3): 279-286.

25. Dunnill MS. Quantitative Methods in the Study of Pulmonary Pathology. *Thorax* 1962: 17: 320-328.

26. Vanoirbeek JA, Rinaldi M, De Vooght V, Haenen S, Bobic S, Gayan-Ramirez G, Hoet PH, Verbeken E, Decramer M, Nemery B, Janssens W. Noninvasive and invasive pulmonary function in mouse models of obstructive and restrictive respiratory diseases. *Am J Respir Cell Mol Biol* 2009: 42(1): 96-104.

27. Marcos V, Zhou Z, Yildirim AO, Bohla A, Hector A, Vitkov L, Wiedenbauer EM, Krautgartner WD, Stoiber W, Belohradsky BH, Rieber N, Kormann M, Koller B, Roscher A, Roos D, Griese M, Eickelberg O, Doring G, Mall MA, Hartl D. CXCR2 mediates NADPH oxidase-independent neutrophil extracellular trap formation in cystic fibrosis airway inflammation. *Nat Med*: 16(9): 1018-1023.

28. Cardoso WV. Lung Morphogenesis, Role of Growth Factors and Transcription Factors. *In:* Harding R, Pinkerton KE, Plopper CG, eds. The Lung: Development, Aging and the Environment. Elsevier, 2004; pp. 3-11.

29. Heussel CP, Herth FJ, Kappes J, Hantusch R, Hartlieb S, Weinheimer O, Kauczor HU, Eberhardt R. Fully automatic quantitative assessment of emphysema in computed tomography: comparison with pulmonary function testing and normal values. *Eur Radiol* 2009: 19(10): 2391-2402.

30. Cobos-Correa A, Trojanek JB, Diemer S, Mall MA, Schultz C. Membrane-bound FRET probe visualizes MMP12 activity in pulmonary inflammation. *Nat Chem Biol* 2009: 5(9): 628-630.

31. Schubert SC, Trojanek JB, Diemer S, Cobos-Correa A, Zhou Z, Treis D, Dai L, Schatterny J, Hirtz S, Schultz C, Mall MA. Airways surface liquid depletion causes MMP-12 dependent emphysema in βENaC-overexpressing mice [Abstract]. *J Cyst Fibros* 2009: 8: 53.

32. Gaggar A, Hector A, Bratcher PE, Mall MA, Griese M, Hartl D. The role of matrix metalloproteases in cystic fibrosis lung disease. *Eur Respir J* 2011: in press.

33. Ford NL, Thornton MM, Holdsworth DW. Fundamental image quality limits for microcomputed tomography in small animals. *Med Phys* 2003: 30(11): 2869-2877.

34. Quintana HK, Cannet C, Schaeublin E, Zurbruegg S, Sugar R, Mazzoni L, Page CP, Fozard JR, Beckmann N. Identification with MRI of the pleura as a major site of the acute inflammatory effects induced by ovalbumin and endotoxin challenge in the airways of the rat. *Am J Physiol Lung Cell Mol Physiol* 2006: 291(4): L651-657.

35. Quintana HK, Cannet C, Zurbruegg S, Ble FX, Fozard JR, Page CP, Beckmann N. Proton MRI as a noninvasive tool to assess elastase-induced lung damage in spontaneously breathing rats. *Magn Reson Med* 2006: 56(6): 1242-1250.

36. Bartling SH, Stiller W., Semmler W., Kiessling F. Small Animal Computed Tomography Imaging. *Current Medical Imaging Reviews* 2007: 3(1): 45-59.

37. Drangova M, Ford NL, Detombe SA, Wheatley AR, Holdsworth DW. Fast retrospectively gated quantitative four-dimensional (4D) cardiac micro computed tomography imaging of free-breathing mice. *Invest Radiol* 2007: 42(2): 85-94.

38. Evans CM, Williams OW, Tuvim MJ, Nigam R, Mixides GP, Blackburn MR, DeMayo FJ, Burns AR, Smith C, Reynolds SD, Stripp BR, Dickey BF. Mucin is produced by clara cells in the proximal airways of antigen-challenged mice. *Am J Respir Cell Mol Biol* 2004: 31(4): 382-394.

FIGURE LEGENDS

FIGURE 1.

Early tracheal mucus obstruction in βENaC-transgenic (βENaC-TG) mice. a, b, d and e) Multiplanar reconstructions (MPR) in coronal (a) and sagittal (b) plane of the neck of a 5 day old WT mouse showing the larynx with its lateral recessus (1); head (2) and spine (3) (a, b). The MPR of a representative βENaC-TG mouse shows obstruction of the sublaryngeal trachea (arrow) in the coronal (d) and sagittal view (e). The mouse died spontaneously on day 6. Of note, this is an example of how three dimensional reconstruction can help to discriminate between the artificial blurring of the larynx in the WT mouse by partial volume effect from obstruction in the βENaC-TG mouse. c and f) Histology (AB-PAS) showing mucus obstruction of the trachea in a representative βENaC-TG mouse killed at the age of 3 days (f) but not in a WT mouse (c). Scale bar = 1 mm (a – f). g) Longitudinal monitoring of the frequency of narrowing or complete obstruction of the trachea in βENaC-TG mice by VCT. Note that tracheal obstruction was not observed in WT mice. h) Tracheal obstruction in deceased and long-term surviving βENaC-TG mice. Data are shown as percentage of mice with lesion present at each time point, n = 12 - 20 mice per group. * $p < 0.05$ vs. age-matched WT and ‡ $p < 0.05$ vs. age-matched βENaC-TG survivors (Fisher's exact test) (g and h).

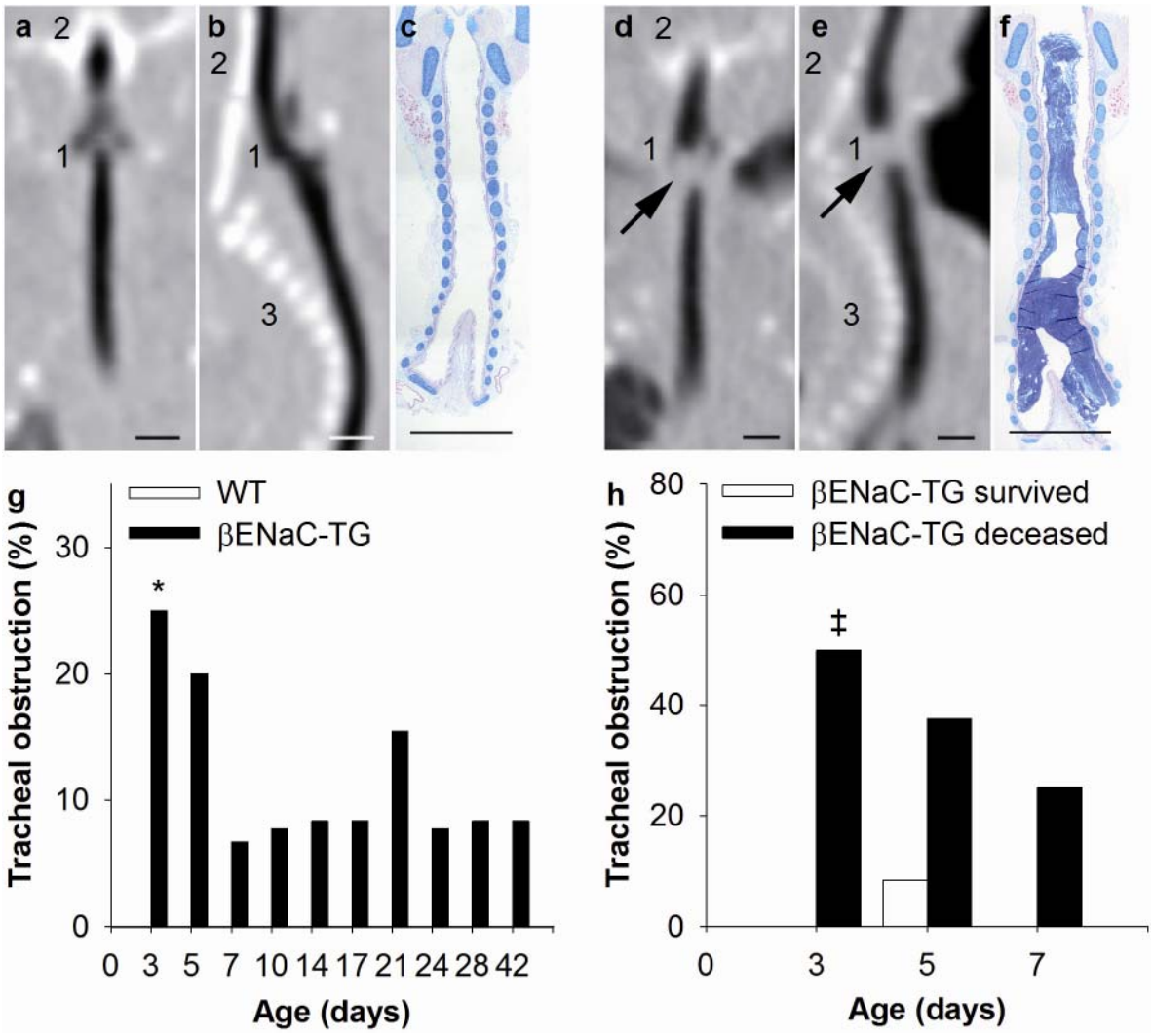

FIGURE 2.

Mucus obstruction in main stem bronchi from wild-type (WT) and βENaC-transgenic (βENaC-TG) mice. a) VCT slice of a WT mouse on day 7. b) Obstruction of the left main stem bronchus (black arrow) in a βENaC-TG mouse on day 7. Images are aligned at the level before the right main stem bronchus enters the lung. Scale bar = 1 mm. c) Summary of longitudinal assessment of mucus obstruction in main stem bronchi in WT and βENaC-TG mice by VCT. Data given as percentage of mice with lesion present, n = 11 – 20 mice per group,* $p < 0.01$ vs. age-matched WT (Fisher's exact test). d - g) Representative airway histology (AB-PAS) from βENaC-TG mice (e and g) and WT (d and f) littermates killed at the age of 2 weeks (d and e) and 6 weeks (f and g), respectively. Lungs were sectioned at the level of the proximal main axial airway near the hilus showing transient goblet cell metaplasia

and intraluminal mucus in 2-week-old (d) but not 6-wwek-old WT mice (f), and persistent mucus obstruction in βENaC-TG mice (e and g). Scale bar = 100 µm. h) Mucus content in the proximal airways. Data are shown as median ± SEM, n = 5 - 9 mice per group, * $p < 0.017$ vs. age-matched WT (Bonferroni-corrected Mann-Whitney-U test), ‡ $p < 0.05$ vs. mice of same genotype day 3 and § $p < 0.05$ vs. mice of same genotype day 14 (Kruskal-Wallis ANOVA with post-hoc Dunn's method).

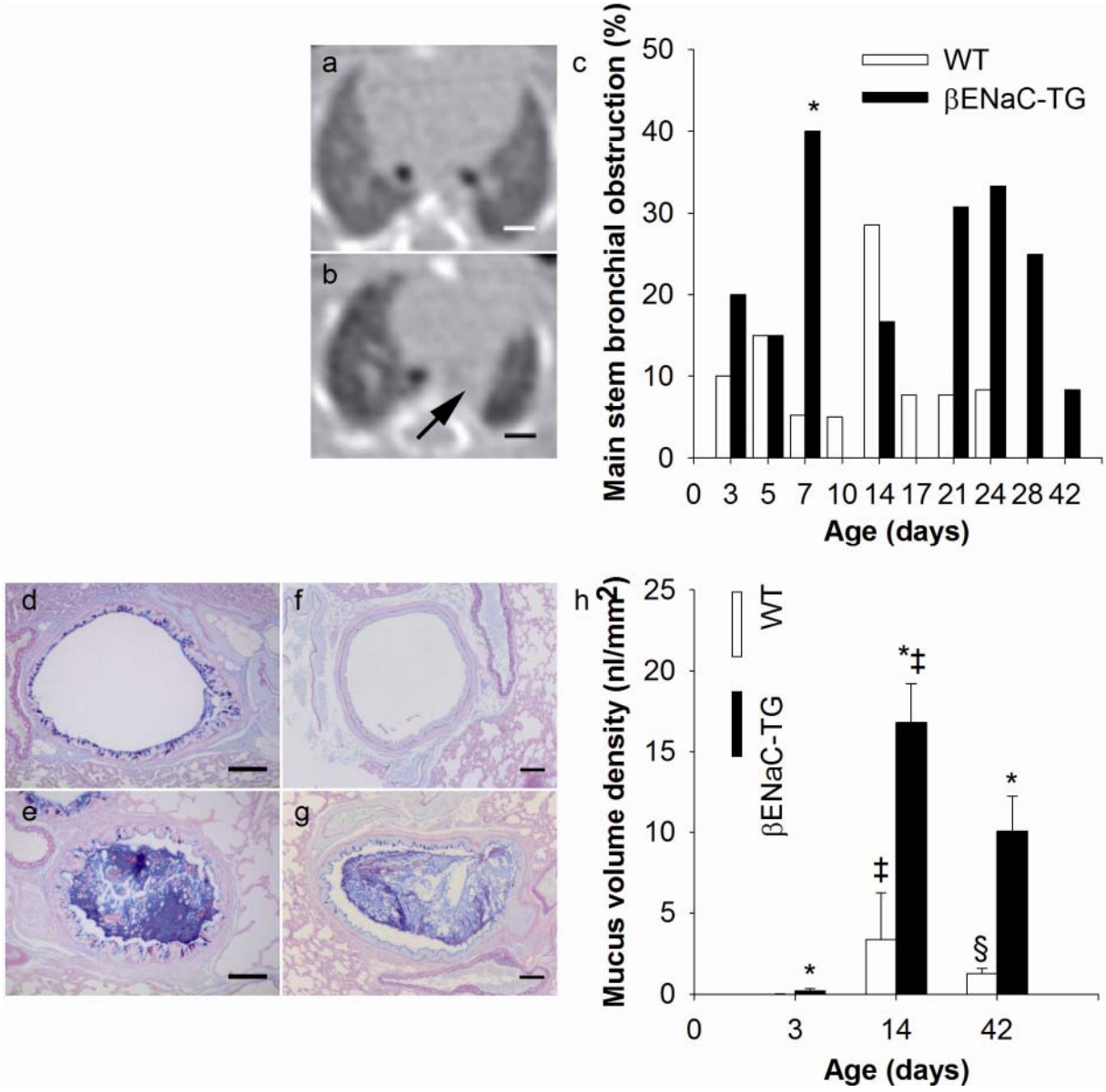

FIGURE 3.

Representative longitudinal VCT images of the chest of wild-type (WT) and βENaC-transgenic (βENaC-TG) mice. VCT images of the lung were taken sequentially starting at the

age of 3 days in a WT mouse (left column), a surviving βENaC-TG littermate (middle column), and a βENaC-TG mouse that died spontaneously on day 21 (right column). Note the development of an overall inhomogeneous lung parenchyma in βENaC-TG mice compared to the homogeneous texture in the WT mouse, and a difference in emphysema severity in the two βENaC-TG mice. These images also give examples of other characteristic pathologies, such as diffuse infiltrates (white arrow), atelectasis (black arrow), as well as air-trapping (white arrowhead). Corresponding Hounsfield Units for each mouse are given at the top of each image. Images were aligned at the level of the branching of the right inferior lobe bronchus. Scale bar = 1 mm. Drawing identifies landmark structures of the mouse chest: heart (1), spine (2), chest wall with costae (3), bronchovascular branches (4), and lung parenchyma (5).

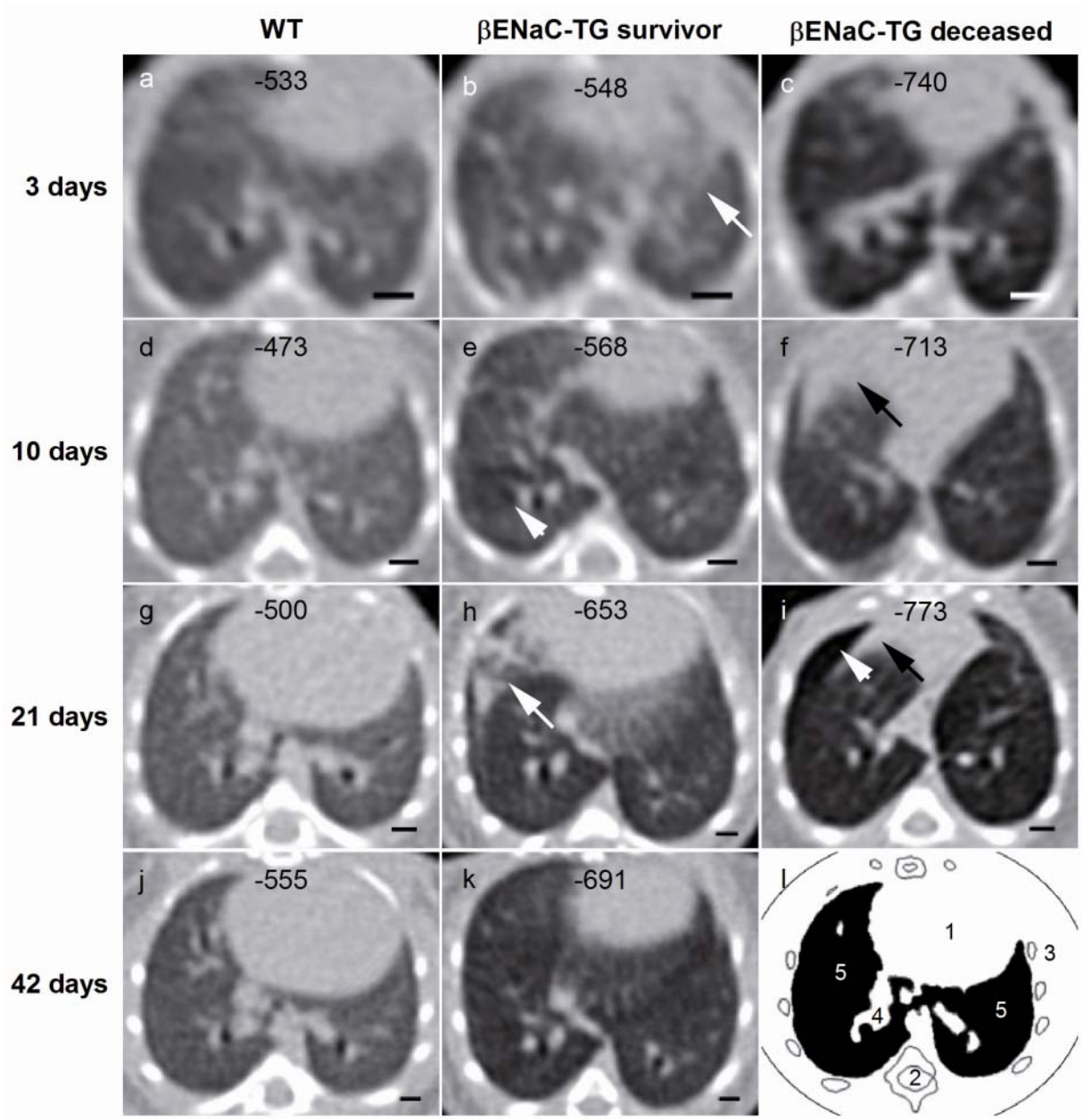

FIGURE 4.

Occurrence of diffuse pulmonary infiltrates and atelectasis from neonatal to adult ages in βENaC-transgenic (βENaC-TG) mice and wild-type (WT) littermates. a) VCT slice at the level of the branching of the inferior lobe bronchus in a 7-day-old WT mouse. b) 3-day-old βENaC-TG mouse with diffuse infiltrates, predominantly of the right thorax (white arrow). c) Morphologically changed diffuse infiltrates (white arrow) and atelectasis of the intermediate lobe (black arrow) in the same βENaC-TG mouse as in b) observed on day 7. d) Note the opacity of the left lung including the bronchus (black arrow) and emphysema of the right lung

in a long-term surviving βENaC-TG mouse observed on day 21. Images were selected to represent relevant pathologies (b – d). Scale bar = 1 mm. e and f) Frequency of diffuse infiltrates (e) and atelectasis (f) in βENaC-TG compared to WT mice. Data are given as percentage of mice with lesion present, n = 11 - 20 mice per group, * $p < 0.001$ and § $p < 0.05$ vs. age-matched WT (Fisher's exact test).

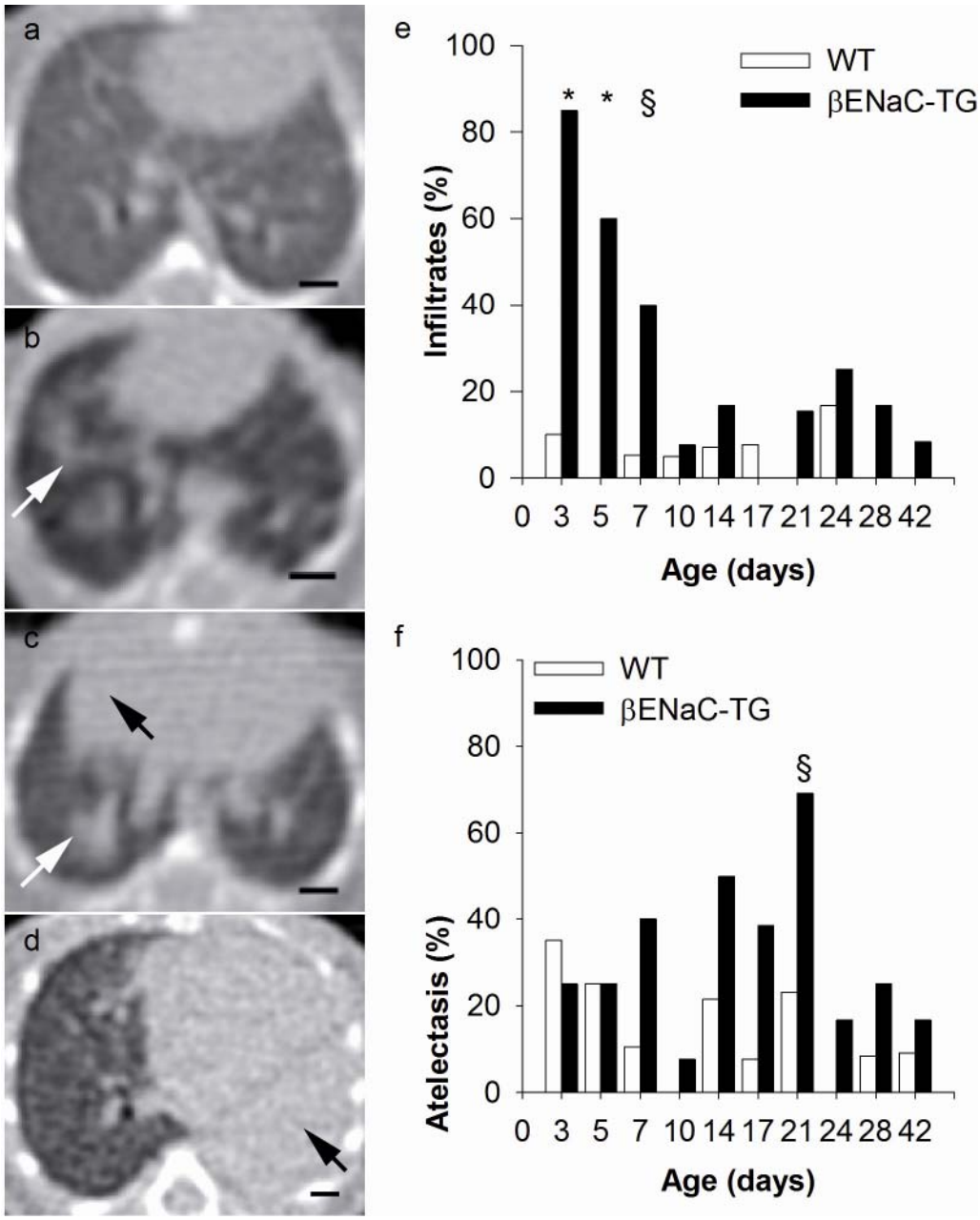

FIGURE 5.

Summary of longitudinal assessment for air-trapping and diffuse parenchymal inhomogeneity in βENaC-transgenic (βENaC-TG) and wild-type (WT) mice. a) Percentage of βENaC-TG

mice showing air-trapping. Note that air-trapping was not observed in WT mice. b) Inhomogeneous lung parenchyma was found in most βENaC-TG mice, but was rarely detected in WT littermates. Data are given as percentage of mice with lesion present. n = 11 – 21 mice per group. * $p < 0.05$ and ‡ $p < 0.005$ vs. age-matched WT (Fisher's exact test and Bonferroni-corrected Fisher's exact test, respectively).

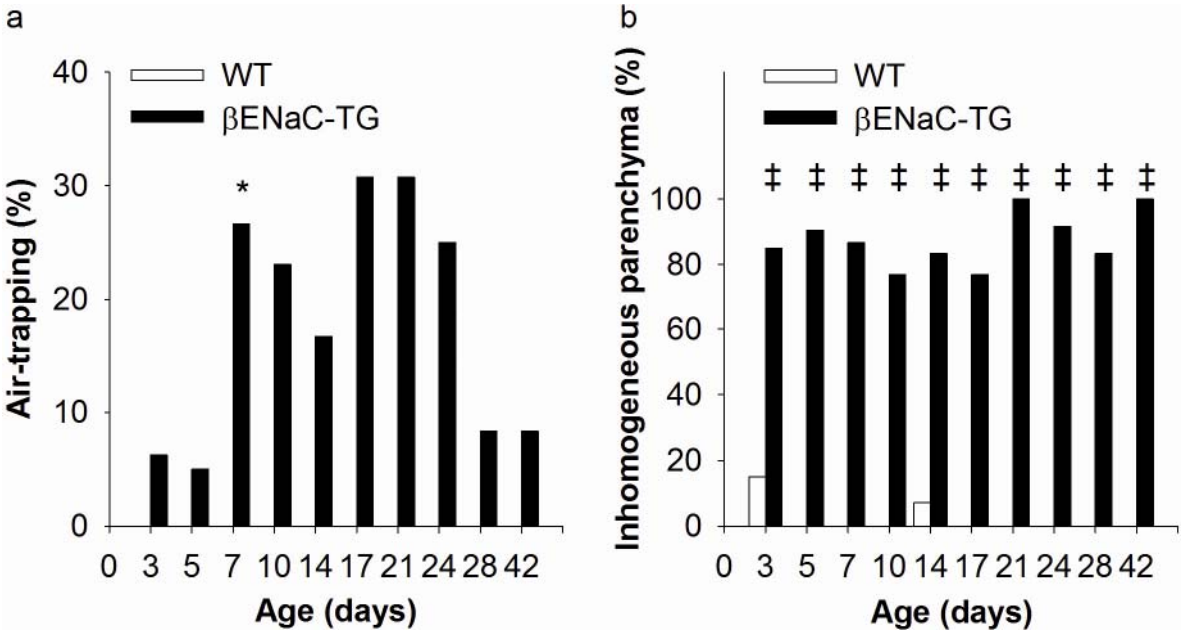

FIGURE 6.

Development of emphysema in βENaC-transgenic (βENaC-TG) mice. a) Summary of longitudinal measurements of the density of lung parenchyma, as determined from Hounsfield Units (HU), in neonatal to adult wild-type (WT) and βENaC-TG mice. Data given as box-plots of the measured HU, the central line shows the median, boxes represent the 25th and 75th percentiles and whiskers mark 10th and 90th percentiles. n = 11 – 20 mice per group. * $p < 0.005$ vs. age-matched WT (Bonferroni-corrected Mann-Whitney-U test), ‡ $p < 0.05$ vs. WT day 3, § $p < 0.05$ vs. WT day 42, and ‖ $p < 0.05$ vs. βENaC-TG day 42 (Kruskal-Wallis ANOVA with post-hoc Dunn's method). b and c) Representative lung histology (H&E) form 2-week-old mice showing enlargement of alveoli in βENaC-TG (c) compared with wild-type WT mice (b). Scale bar = 100 µm. d) Mean linear intercepts were determined in WT and βENaC-TG mice at the age of 3 days, 2 weeks and 6 weeks. Data are shown as mean ±

SEM. n = 5 - 8 mice per group, * $p < 0.017$ vs. age-matched WT (Bonferroni-corrected Student's t-test), ‡ $p < 0.001$ vs. WT day 3 and § $p < 0.01$ vs. βENaC-TG day 3 (one way ANOVA with post-hoc Bonferroni-corrected Student's t-test). e and f) Total lung capacity (e) and pressure-volume curves (f) were determined in 6-week-old βENaC-TG mice and WT littermates. Data are show as mean ± SEM. n = 18 - 20 per group, * $p < 0.01$ vs. corresponding WT (Bonferroni-corrected Student's t-test); ‡ $p < 0.05$ vs. WT (Student's t-test).

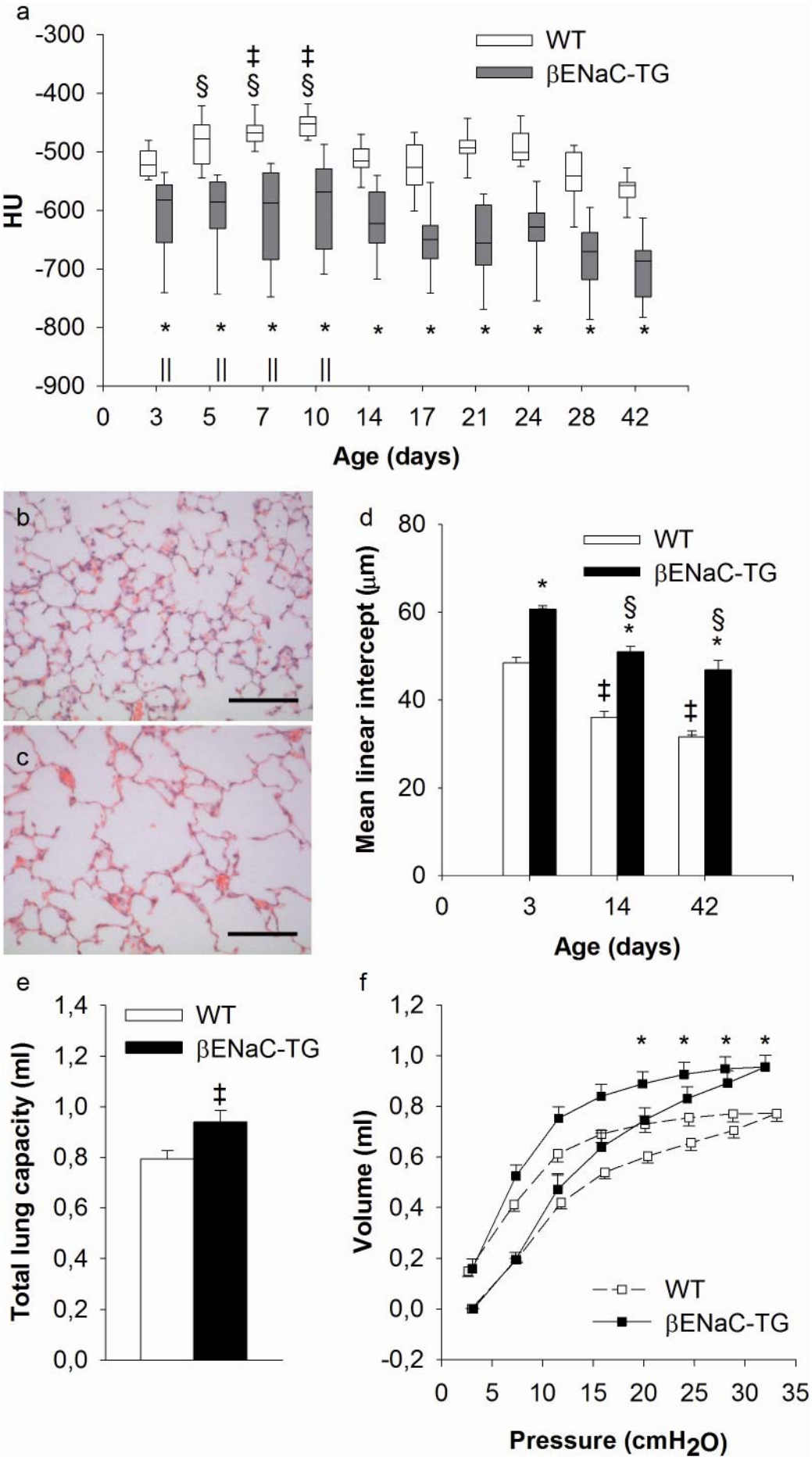
a
HU
-300
-400
-500
-600
-700
-800
-900
WT
βENaC-TG
0 3 5 7 10 14 17 21 24 28 42
Age (days)
b
c
d
Mean linear intercept (μm)
80
60
40
20
0
WT
βENaC-TG
0 3 14 42
Age (days)
e
Total lung capacity (ml)
1,4
1,2
1,0
0,8
0,6
0,4
0,2
0,0
WT
βENaC-TG
f
Volume (ml)
1,2
1,0
0,8
0,6
0,4
0,2
0,0
-0,2
WT
βENaC-TG
0 5 10 15 20 25 30 35
Pressure (cmH2O)

FIGURE 2 online supplement.

Mucus obstruction in main stem bronchi from wild-type (WT) mice. VCT slice of a WT mouse on day 14 which depicts subtotal narrowing of the left main stem bronchus (black arrow). The image is aligned at the level before the right main stem bronchus enters the lung. Scale bar = 1 mm.